Eur J Nucl Med Mol Imaging (2009) 36:1235–1244
DOI 10.1007/s00259-009-1096-y

ORIGINAL ARTICLE

^{124}I-L19-SIP for immuno-PET imaging of tumour vasculature and guidance of ^{131}I-L19-SIP radioimmunotherapy

Bernard M. Tijink · Lars R. Perk · Marianne Budde · Marijke Stigter-van Walsum · Gerard W. M. Visser · Reina W. Kloet · Ludger M. Dinkelborg · C. René Leemans · Dario Neri · Guus A. M. S. van Dongen

Received: 7 January 2009 / Accepted: 9 February 2009 / Published online: 4 March 2009

Abstract
Purpose The human monoclonal antibody (MAb) fragment L19-SIP is directed against extra domain B (ED-B) of fibronectin, a marker of tumour angiogenesis. A clinical radioimmunotherapy (RIT) trial with ^{131}I-L19-SIP was recently started. In the present study, after GMP production of ^{124}I and efficient production of ^{124}I-L19-SIP, we aimed to demonstrate the suitability of ^{124}I-L19-SIP immuno-PET for imaging of angiogenesis at early-stage tumour development and as a scouting procedure prior to clinical ^{131}I-L19-SIP RIT.
Methods ^{124}I was produced in a GMP compliant way via ^{124}Te(p,n)^{124}I reaction and using a TERIMO™ module for radioiodine separation. L19-SIP was radioiodinated by using a modified version of the IODO-GEN method. The biodistribution of coinjected ^{124}I- and ^{131}I-L19-SIP was compared in FaDu xenograft-bearing nude mice, while ^{124}I PET images were obtained from mice with tumours of <50 to ~700 mm^3.
Results ^{124}I was produced highly pure with an average yield of 15.4±0.5 MBq/μAh, while separation yield was ~90% efficient with <0.5% loss of TeO_2. Overall labelling efficiency, radiochemical purity and immunoreactive fraction were for ^{124}I-L19-SIP: ~80 , 99.9 and >90%, respectively. Tumour uptake was 7.3±2.1, 10.8±1.5, 7.8±1.4, 5.3±0.6 and 3.1±0.4%ID/g at 3, 6, 24, 48 and 72 h p.i., resulting in increased tumour to blood ratios ranging from 6.0 at 24 h to 45.9 at 72 h p.i.. Fully concordant labelling and biodistribution results were obtained with ^{124}I- and ^{131}I-L19-SIP. Immuno-PET with ^{124}I-L19-SIP using a high-resolution research tomograph PET scanner revealed clear delineation of the tumours as small as 50 mm^3 and no adverse uptake in other organs.
Conclusions ^{124}I-MAb conjugates for clinical immuno-PET can be efficiently produced. Immuno-PET with ^{124}I-L19-SIP appeared qualified for sensitive imaging of tumour neovasculature and for predicting ^{131}I-L19-SIP biodistribution.

Keywords PET imaging · L19-SIP · Extra domain B of fibronectin · Angiogenesis · Radioimmunotherapy

Bernard M. Tijink and Lars R. Perk contributed equally to this article.

B. M. Tijink · L. R. Perk · M. Budde · M. Stigter-van Walsum · C. R. Leemans · G. A. M. S. van Dongen (✉)
Department of Otolaryngology/Head and Neck Surgery,
VU University Medical Center,
De Boelelaan 1117, P.O. Box 7057, 1007 MB Amsterdam,
The Netherlands
e-mail: gams.vandongen@vumc.nl

G. W. M. Visser · R. W. Kloet · G. A. M. S. van Dongen
Nuclear Medicine & PET Research,
VU University Medical Center,
Amsterdam, The Netherlands

L. M. Dinkelborg
Global Drug Discovery, Bayer Schering Pharma AG,
Berlin, Germany

D. Neri
Institute of Pharmaceutical Sciences,
Swiss Federal Institute of Technology,
Zurich, Switzerland

Introduction

Angiogenesis is one of the hallmarks of cancer, and therefore, considerable efforts have been made recently to image as well as to eradicate tumour vasculature, preferably in a combined fashion [1, 2]. One of the appealing targets for both approaches is the splice variant of fibronectin containing extra domain B (ED-B). ED-B is abundantly

expressed around the vasculature of a variety of human cancers, primary tumours as well as metastases [3–6]. Interestingly, ED-B is undetectable in normal tissues, with the exception of tissues undergoing physiological modelling (e.g. endometrium and ovary) and during wound healing [3]. This target is highly conserved in different species, having 100% homology in many mammalian species (e.g. human, rat, mouse), and therefore making proof of principle studies in tumour-bearing mice of special relevance [7].

Recently, a human recombinant scFv fragment directed against ED-B, designated L19, was developed [8]. Using its variable regions, several other L19 formats were constructed, including dimeric scFv [$(scFv)_2$], a human bivalent "small immunoprotein" (SIP, ~80 kDa), and a complete human IgG1 [9]. Radiolabelled L19 constructs have been evaluated in tumour-bearing nude mice to identify the most appropriate conjugate for radioimmunotherapy (RIT) of solid tumours [9–12]. To this end, the L19 derivatives were labelled with ^{125}I or ^{111}In [10]. The resulting biodistribution data were used to perform dosimetry for the corresponding therapeutic counterparts labelled with ^{131}I and ^{90}Y, respectively, and to select a conjugate for clinical RIT. The most favourable therapeutic index was found for ^{131}I-L19-SIP, while this index was a poor one for ^{90}Y-labelled derivatives [10]. RIT with ^{131}I-L19-SIP at maximum tolerated dose caused significant tumour growth delay and improved survival in several animal models [10–12].

On the basis of the aforementioned bright perspectives, a clinical RIT trial with ^{131}I-L19-SIP was designed [13]. This trial comprises the selection of RIT candidate patients on the basis of pretherapy SPECT imaging and dosimetry. Rationales for this approach are the variable ED-B expression in tumours, with higher expression in the more aggressive ones, and the potential occurrence of ED-B expression in normal tissues.

We and others recently proposed immuno-PET as a high-resolution quantitative imaging procedure before or concomitant with RIT to improve confirmation of tumour targeting and to assess radiation dose delivery to both tumours and normal tissues [14–16]. Important in such approach is the choice of the positron emitting radionuclide to be used for radiolabelling. Among others, its physical half-life ($t_{1/2}$) should be compatible with the time needed for a MAb to achieve optimal tumour to non-tumour ratios, being >24 h for L19-SIP. In addition, when immuno-PET is used for selection of RIT candidates, the radioimmunoconjugates used for immuno-PET and RIT should demonstrate a similar biodistribution, and therefore, by preference, radionuclides with comparable in vivo behaviour must be used. The starting positron emitter solution should meet appropriate radiopharmaceutical quality standards when used for clinical purposes.

The halogens ^{76}Br ($t_{1/2}$=16.2 h) and ^{124}I ($t_{1/2}$=4.18 d) are promising candidate positron emitters for L19-SIP immuno-PET in combination with ^{131}I-L19-SIP RIT; however, availability of GMP-compliant material is a problem for both. Rossin et al. [17] recently described ^{76}Br-L19-SIP for imaging of tumour neovasculature in xenograft-bearing nude mice. While tumour uptake of ^{76}Br-L19-SIP was high, a disadvantage was the long retention of radioactivity in blood and the very slow renal excretion. As a consequence, the background activity in non-target organs was higher than that reported for ^{125}I-labelled L19-SIP, and this resulted in lower target to non-target ratios.

Taking the aforementioned aspects into account, we hypothesized that ^{124}I-L19-SIP might be the most optimal candidate for immuno-PET imaging of tumour neovasculature, and for prediction of biodistribution and dosimetry of ^{131}I-L19-SIP in RIT. Although the choice of ^{124}I-L19-SIP immuno-PET seems logical, no such studies have been reported as yet, and several technical hurdles had to be taken to enable future clinical evaluation. For this purpose, and to facilitate the translation to clinical application, we developed the production and purification of ^{124}I in a GMP-compliant setting, and its coupling to L19-SIP, with the aid of IODO-GEN. With respect to the latter, procedures were established for efficient coupling of no-carrier-added ^{124}I. ^{124}I-L19-SIP was evaluated by comparison of biodistribution with ^{131}I-L19-SIP upon coinjection in xenograft-bearing nude mice and by imaging of mice with tumours of <50 to ~700 mm^3 with a high-resolution research tomograph (HRRT) PET scanner.

Materials and methods

Monoclonal antibody, xenograft line and radioactivity

Antibody L19-SIP (conc. 1.23 mg/ml), directed against the ED-B domain of fibronectin, was obtained from Bayer Schering Pharma, Berlin, Germany. Selection, construction and production of L19-SIP (MW=~80 kD) have been described previously [8, 9]. The MAb cetuximab (Erbitux® conc. 2.0 mg/ml) was used as reference for optimization of ^{124}I labelling and was purchased from Merck, Darmstadt, Germany.

The human HNSCC cell line FaDu has been described before [18], was obtained from KH Heider (Boehringer Ingelheim Austria), and has been characterized for ED-B expression [11].

^{131}I (66.4 GBq/ml; specific activity 611 GBq/mg) was purchased from Perkin Elmer.

^{124}I production and quality tests

^{124}I was produced at BV Cyclotron VU (Amsterdam, The Netherlands) via a ^{124}Te(p,n)^{124}I reaction and isolated by

use of dry distillation essentially as described by Qaim et al. [19]. In short, the target consisted of a glassy layer of $^{124}TeO_2$ (enrichment of 99.8%; Isoflex, San Francisco, CA, USA) mixed with 5% (w/w) Al_2O_3. The physical thickness of the target was 250 mg/cm^2. A platinum (Pt) disc (Ø= 25 mm; thickness=2 mm) containing a cavity (Ø=14 mm; depth=1 mm) was used as backing. The target was loaded on an in house made solid target station installed on a IBA Cyclone 18/9 cyclotron and irradiated with 12.5 MeV protons using a beam current of up to 20 μA for 2–10 h. During irradiation, the target was cooled in front using helium cooling and at the back using water cooling. A TERIMO module (Elex Commerce, Belgrade, Serbia) was used for radioiodine separation by dry distillation. Trapping of ^{124}I was performed in 1 ml 50 mM NaOH.

Assessment of the radiochemical purity of the ^{124}I preparations was performed by HPLC analysis, using a LiChrospher 100 RP-18 column (125×4 mm, 5 μm; Merck). As eluent 0.1 mol/l NaCl/0.004 mol/l octylamine (pH 7) + 5% (v/v) MeCN was used at a flow rate of 1.5 ml/min. The HPLC retention times were 1.5 min for IO^{3-} and 5.0 min for I^- [20]. For identification and quantification of radionuclidic contaminants a germanium(lithium) [Ge(Li)] detector was used coupled to a multichannel analyser [21]. The tellurium content was assessed by a spectrophotometric method as described by Qui-e et al. [22]. The endotoxin levels were assessed by use of an FDA-licensed LAL test system according to the instructions provided by the supplier (Endosafe®-PTS, Charles River, Charleston, SC, USA). Autoclaving was not performed but can be used as an option to assure sterility.

Radiolabelling

Preparation of ^{124}I-L19-SIP Three sets of labelling experiments with L19-SIP were performed within the following general frame [23]: 20 ml ß-scintillation glass vials were coated with 25 μg IODO-GEN (Pierce, Rockford, IL, USA) in dichloromethane, dried under a stream of N_2 gas, resulting in a thin coating of IODO-GEN on the bottom surface of the vial. The vials were stored under N_2 atmosphere. To a IODO-GEN-coated glass vial, successively 50 μl 0.5 M Na_2HPO_4 (pH 7.4), 450-X-Y μl 0.1 M Na_2HPO_4 (pH 6.8), X μl L19-SIP and Y μl radioiodine solution were added. After gentle shaking for 4 min at room temperature, 0.1 ml ascorbic acid (25 mg/ml, pH 5) was added to reduce the IODO-GEN and to protect the L19-SIP against radiation damage. After an additional 5 min, the reaction mixture was transferred to a syringe connected to a filter (0.22 μm Acrodisc, Gelman Sciences, Ann Arbor, MI, USA) followed by 0.4 ml 0.1 M Na_2HPO_4 (pH 6.8), used for an additional rinsing of the reaction vial. This combined solution was filtered and purified on a PD-10 column (GE Healthcare Life Sciences, Piscataway, NJ, USA) with 0.9% NaCl/ascorbic acid (5 mg/ml, pH 5) as eluent. The first 2.5 ml (1.0 ml sample volume and the first 1.5 ml) were discarded and the radiolabelled antibody was collected in the next 1.5 ml.

In the first set, the ^{124}I labelling efficiency was optimized by varying the amount of NaI present during the reaction. In these experiments X was 82 μl (100 μg, 1.33 nmol) L19-SIP, while Y was 50 μl of a series of pre-equilibrated (5 min) ^{124}I/NaI mixtures, each containing 2.4 MBq ^{124}I and, respectively, 6700, 1675, 838, 419, 209, 105, 52, 26 and 0 pmol NaI. A similar series of labellings was performed with the control MAb cetuximab, for which X was 50 μl (100 μg, 0.66 nmol). It is of note that the 2.4 MBq ^{124}I activity used in each reaction in the case of carrier-free ^{124}I corresponds with 2.1 pmol iodine.

In the second set, ^{124}I-L19-SIP and ^{131}I-L19-SIP were synthesized for a biodistribution study. The labelling was carried out with X=163 μl (200 μg, 2.66 nmol) L19-SIP; Y was 83 μl ^{124}I solution (14.8 MBq, 266 pmol NaI). For ^{131}I, X was also 163 μl L19-SIP solution, and Y was 2 μl of a diluted ^{131}I batch (14.8 MBq). No NaI carrier was added to this solution, because 14.8 MBq ^{131}I already corresponds with 190.7 pmol ^{127}I and 61.4 pmol ^{131}I.

In the third set, ^{124}I-L19-SIP was synthesized for PET studies. The labelling was carried out with X is 142 μl (175 μg, 2.33 nmol) L19-SIP; Y was 90 μl ^{124}I solution (38.5 MBq, 232 pmol NaI).

Analyses

All conjugates were analysed by instant thin-layer chromatography (ITLC) and HPLC, by SDS-polyacrylamide gel electrophoresis (PAGE) followed by phosphor imager analysis for integrity, and by a cell-binding assay for immunoreactivity.

HPLC monitoring of the final product was performed on a Jasco HPLC system using a Superdex™ 200 10/300 GL size exclusion column (GE Healthcare Life Sciences, Piscataway, NJ, USA). As eluent a mixture of 0.05 M sodium phosphate and 0.15 M sodium chloride (pH 6.8) was used at a flow rate of 0.5 ml/min.

ITLC analysis of radiolabelled antibodies was carried out on silica gel-impregnated glass fibre sheets (Gelman Sciences, Ann Arbor, MI, USA). As mobile phase, 20 mM citrate buffer, pH 5.0 was used. The integrity of the radioimmunoconjugates was monitored by electrophoresis on a Phastgel System (Pharmacia Biotech, Piscataway, NJ, USA), using preformed high-density SDS-PAGE gels under non-reducing conditions. Analysis and quantification of the radioactivity in the bands was performed with the use of Phosphor Imager screens and subsequent scanning by a Phosphor Imager (B&L-Isogen Service Laboratory, Amsterdam, The Netherlands).

In vitro binding characteristics of radiolabelled L19-SIP were determined in an immunoreactivity assay essentially as described before [11], using ED-B-coated Sepharose resin in phosphate-buffered saline (PBS) containing 1% bovine serum albumin (BSA). Five serial dilutions, ranging from 100 to 6.2 μl resin per tube, were prepared in triplicate in PBS/1% BSA. L19-SIP (125 ng), labelled with ^{124}I or ^{131}I, was added to the tubes and the samples were incubated overnight at 4°C for binding. Excess unlabelled L19-SIP antibody (10 μg per tube) was added to a second set of tubes with the lowest concentration of resin to determine non-specific binding. After incubation, resin was spun down and radioactivity in the pellet and supernatant was determined in a gamma counter and the percentage bound and free radioactivity was calculated. Binding data were graphically analysed in a modified Lineweaver-Burk plot and the immunoreactive fraction was determined by linear extrapolation to conditions representing infinite antigen excess.

Biodistribution studies

For the biodistribution experiments with L19-SIP, nude mice bearing the subcutaneously implanted human head and neck squamous cell carcinoma (HNSCC) xenograft line FaDu were used. No control SIP constructs were included in the current evaluations, because previous studies had shown the specificity of L19-SIP for targeting of ED-B-expressing tumours in a direct comparison with the control D1.3-SIP directed against hen egg white lysosyme [9]. Female mice (Hsd athymic *nu/nu*, 25–32 g; Harlan CPB) were 8–10 weeks old at the time of the experiments. Animal experiments were performed according to National Institutes of Health principles of laboratory animal care and Dutch National Law (*Wet op de dierproeven*, Stb 1985, 336).

At t=0, FaDu-bearing nude mice (n=20) received 25 μg of L19-SIP including 0.37 MBq of ^{124}I-labelled format and 0.37 MBq of ^{131}I-labelled format, by i.v. injection in the retro-orbital plexus. Two days before the experiments, 0.1% of potassium iodide was added to the drinking water to block thyroid uptake of ^{124}I/^{131}I. For assessment of biodistribution, four mice containing two tumours each were sacrificed at 3, 6, 24, 48 and 72 h after injection. All animals were anaesthetized, bled, killed and dissected. Besides the tumours, the following organs were removed: tongue, sternum, heart, lung, liver, spleen, kidney, bladder, muscle, colon, ileum and stomach. Also stomach contents were retained. After blood, tumour, normal tissues and stomach contents were weighed, the amount of radioactivity in each was counted in a gamma counter (Wallac LKB-CompuGamma 1282, Kabi Pharmacia, Woerden, The Netherlands), using the corresponding window settings for ^{124}I and ^{131}I (for the 603 keV and 364 keV gamma energy, respectively). In this dual-isotope biodistribution study, cross-over corrections from one radionuclide into the alternate window were automatically performed using a standard of each radionuclide. Radioactivity uptake was calculated as the percentage of the injected dose per gram of tissue (%ID/g), corrected for radioactive decay.

The mean tumour size of eight tumours at dissection was 234±204, 384±192, 273±144, 371±213 and 315±201 mm^3 for the groups to be dissected at 3, 6, 24, 48 and 72 h after injection, respectively.

PET imaging procedures

Two animal PET studies for imaging of tumour targeting with ^{124}I-L19-SIP were performed essentially as described by Verel et al. [21]. During scanning mice were placed on a temperature controlled animal bed. In the first experiment, but not in the second experiment, 0.1% of potassium iodide was added to the drinking water to block thyroid uptake of ^{124}I. PET studies were performed using a double crystal layer HRRT PET scanner (Siemens/CTI, Knoxville, TN, USA), a dedicated small animal and human brain scanner [24] with a spatial resolution transaxial between 2.3 and 3.2 full-width at half-maximum (FWHM) and in axial direction between 2.5 and 3.4 FWHM. A detailed description of the performance of the scanner and the software is given by De Jong et al. [24]. Transmission scans for attenuation and scatter correction were routinely obtained with each scan in two-dimensional mode using a single point ^{137}Cs source. Three-dimensional emission scans were acquired in 64-bit list mode during 60 min using a 400–650 keV window. The 64-bit list mode file was first converted into a single-frame sinogram using a span of 9, and subsequently reconstructed using a 3-D ANW-OSEM reconstruction with 2 iterations and 16 subsets and matrix size 256×256 including corrections for normalization, decay and dead time. 3-D ANW-OSEM is a 3-D attenuation and normalization weighted ordered subset expectation maximalization reconstruction [25].

In a first PET imaging study, three FaDu xenograft-bearing nude mice were injected i.v. with 3.7 MBq ^{124}I-L19-SIP (25 μg). The mean tumour size at the start of the experiment was 266±158 mm^3. During scanning at 1 and 2 days p.i., the animals were sedated using isoflurane.

Because of clear tumour visualization in the first experiment, a second PET imaging experiment was performed to determine at which stage of tumour development tumours can be readily imaged by ^{124}I-L19-SIP immuno-PET. To this end, at 1, 2 and 3 weeks after subcutaneous tumour implantation, six mice were injected i.v. with 3.7 MBq ^{124}I-L19-SIP (25 μg) and imaged 48 h after each injection. Before each PET imaging procedure, the size of the tumours was measured with callipers. Because of inaccurate measurement of tumour smaller than 50 mm^3, size of these tumours was indicated to be <50 mm^3.

Statistics

Differences in tissue uptake between coinjected conjugates were statistically analysed for each time point with Excel 2003 software (Microsoft) using Student's *t* test for paired data. Differences in average tumour volume between the various groups were statistically analysed for each time point with Student's *t* test for unpaired data. Two-sided significance levels were calculated, and $p<0.01$ was considered statistically significant.

Results

GMP-compliant production of ^{124}I

Production of ^{124}I via ^{124}Te(p,n)^{124}I reaction at incident energy of 12.5 MeV resulted in an average target yield ($n=15$) of 15.4±0.5 MBq/μAh at the end of bombardment (EOB). During typical commercial runs, bombardment durations of 8 h at 18 μA resulted in a yield of 2.2 GBq ^{124}I in-target. Subsequent dry distillation resulted in >90% recovery of radioiodine from the TeO_2 target into the 50 mM NaOH solution, while less than 0.5% TeO_2 was lost from the target. To allow for GMP-compliant harvesting of ^{124}I, the TERIMO module was localized in a hot cell integrated in a clean room meeting GMP conditions (GMP grade C). Visual inspection of the final product always revealed a clear, colourless solution. The radiochemical purity as assessed by HPLC analysis was >99.6% (specification for release >95% as iodide). After storage for 11 days, the radiochemical purity was still greater than 99.5%. Three days after production (considered the time of application) the radionuclidic purity was 99.6±0.06%, fulfilling the specification for release (>99.0%). The main radionuclidic contaminants were ^{123}I (<0.5%) and ^{125}I (<0.03%); other radionuclidic impurities, if any, were below detection limit. The tellurium content of the ^{124}I-NaOH solution was 6±1.6 ng/ml (specification for release <1 μg/ml). The endotoxin levels were <1.5 EU/ml (specification for release <5 EU/ml).

Radiolabelling

Despite being >99% in the iodide form, the overall labelling yield of L19-SIP with ^{124}I produced in house was only at around 50%. This low labelling yield is inherent to the fact that ^{124}I is carrier free, and not because the oxidative power of 25 μg vial-coated IODO-GEN is insufficient (25 μg IODO-GEN=57 nmol and corresponds to 228 nmol N-Cl groups). In the presence of the excessive amount of 6.7 nmol NaI the ^{124}I labelling yield was 96% upon using the same amount of L19-SIP (100 μg, 1.33 nmol) and the same amount (25 μg vial-coated) IODO-GEN. For a study on the fine tuning of I/MAb molar ratios, the labelling of L19-SIP was evaluated in relation to the amount of NaI present during labelling. Figure 1 shows that in the presence of 200 pmol NaI or more, the labelling efficiency was 85–95%. It is of note that the same data as shown in Fig. 1 were also obtained when cetuximab was used as a model substrate (data not shown).

For the biodistribution study, the amount of NaI was selected in such a way that the I/MAb of the ^{124}I product was the same as that of the ^{131}I product. As a result, the I/MAb molar ratio of both resulting conjugates was about 1:10. For the subsequent ^{124}I animal PET studies the same I/MAb molar ratio was created. The radiochemical purity of the injected products was 99.9% for ^{124}I-L19-SIP as well as for ^{131}I-L19-SIP. Phosphor imager analysis of SDS-PAGE gels as well as HPLC analysis revealed optimal integrity of the antibody. The immunoreactivity of ^{124}I-L19-SIP was 93.1±4.2% at the highest resin concentration and 100% at infinite antigen excess (for ^{131}I-L19-SIP these figures were 89.6 and 100%, respectively).

Biodistribution in tumour-bearing nude mice

For comparison of the biodistribution of ^{124}I- and ^{131}I-L19-SIP in tumour-bearing nude mice, both conjugates were coinjected. At 3, 6, 24, 48 and 72 h after injection, the average uptake (%ID/g, mean ± SEM) in tumour, blood, normal tissues and gastrointestinal contents was determined and shown in Fig. 2 for a selected panel of tissues. Blood values were similar for both conjugates at all time points, indicating that (1) radiolabelling had not differentially altered the pharmacokinetics of the antibody, and (2) serum stability was comparable for both conjugates. There was no significant difference in uptake of ^{124}I and ^{131}I in the majority of normal organs (differences indicated by asterisk in Fig. 2).

Tumour uptake of ^{124}I was 7.3±2.1, 10.8±1.5, 7.8±1.4, 5.3±0.6 and 3.1±0.4%ID/g tissue at 3, 6, 24, 48 and 72 h

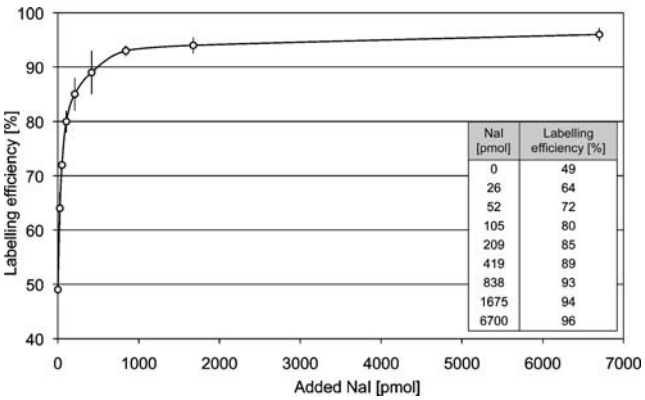

Fig. 1 Labelling of L19-SIP with ^{124}I: labelling efficiency in relation to the amount of NaI carrier added. Labelling efficiency was assessed by ITLC

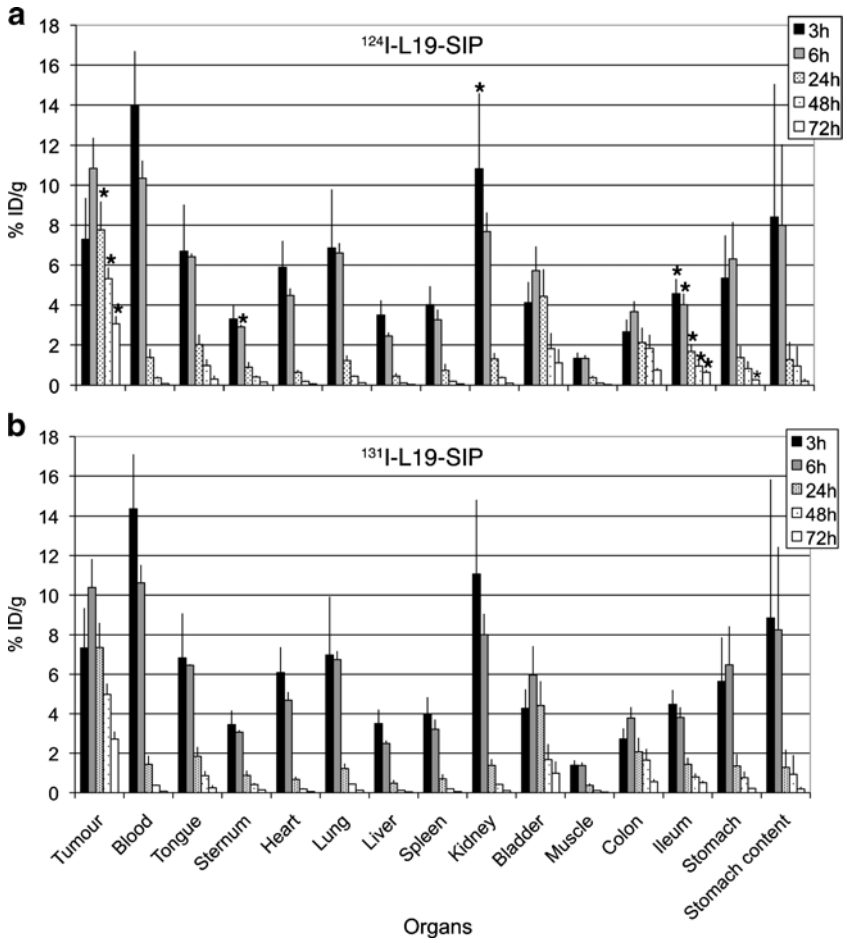

Fig. 2 Biodistribution of coinjected ^{124}I-L19-SIP (0.37 MBq) (**a**) and ^{131}I-L19-SIP (0.37 MBq) (**b**) in FaDu xenograft-bearing nude mice at 3, 6, 24, 48 and 72 h after intravenous injection. Significant differences in uptake of the conjugates are marked with an *asterisk*. Data are presented as average of four animals and standard deviation

p.i.. In comparison, ^{131}I levels at these time points were 7.3±2.0, 10.4±1.4, 7.4±1.2, 5.0±0.5 and 2.7±0.4%ID/g, respectively. From 6 h p.i. onwards, ^{124}I-L19-SIP uptake in tumours was higher than in any normal organ or tissue. During the same period, blood levels decreased from 14.0±2.7%ID/g at 3 h after injection to 0.08±0.03%ID/g at 72 h after injection. This resulted in very favourable tumour to blood ratios at later time points ranging from 6.0 at 24 h p.i. to 45.9 at 72 h p.i. (Table 1). Also tumour to normal tissue ratios were relatively high from 24 h after injection onwards, for most organs exceeding the value 4 (Table 1). Rapid blood clearance during the first 24 h was accompanied by high radioactivity uptake in kidney, stomach and stomach contents. This is indicative of rapid renal excretion and catabolism of the conjugate with partial reabsorption of ^{124}I metabolites, which can accumulate in the stomach and are released from the body via intestines and colon.

PET imaging with ^{124}I-L19-SIP in tumour-bearing nude mice

Immuno-PET with ^{124}I-L19-SIP revealed clear delineation of the tumours at 24 h p.i. (Fig. 3a). In addition, slight uptake was visible in the stomach region, as was previously observed in the biodistribution experiments (Fig. 2). Prominent uptake of radioactivity was also observed in the bladder region, and from this single scan it was not clear whether uptake was due to targeting of ED-B-expressing normal tissues by ^{124}I-L19-SIP (e.g. endometrium and ovary) or due to excretion of ^{124}I-containing catabolites via the urine. Later scans of the same tumour-bearing nude mice at 48 h p.i., however, showed only clear retention of ^{124}I-L19-SIP in the tumours (Fig. 3b). This observation confirms that temporarily high levels of ^{124}I in the stomach regions were related to the presence of catabolites of ^{124}I-L19-SIP and/or free iodine.

Since tumour size in the previous imaging experiment was relatively large, 266±158 mm^3 at the time of conjugate injection, we examined how early after transplantation FaDu tumours can be visualized. To this end, at 1, 2 and 3 weeks after transplantation of the FaDu tumours a freshly produced ^{124}I-L19-SIP sample was injected, and 48 h later an imaging procedure was performed. As illustrated by Fig. 4, tumour delineation was possible from 1 week after implantation onwards, when tumour size was still <50 mm^3.

Table 1 Tumour to normal tissue ratios of coinjected ^{124}I-L19-SIP and ^{131}I-L19-SIP in FaDu xenograft-bearing nude mice

Biodistribution time	3h	6h	24h	48h	72h
Tumour to tissue ratios of ^{124}I-L19-SIP					
Blood	0.49	1.07	6.04	15.00	45.90
Tongue	1.11	1.69	4.14	5.84	14.76
Sternum	2.20	3.74	9.65	13.19	20.37
Heart	1.23	2.43	12.39	28.69	75.36
Lung	1.18	1.65	6.72	12.09	25.61
Liver	2.07	4.44	18.50	46.73	96.01
Spleen	1.80	3.37	11.48	27.95	53.25
Kidney	0.69	1.42	6.15	14.26	31.30
Bladder	1.80	1.96	1.83	3.72	9.99
Muscle	5.49	8.24	22.57	49.97	118.89
Colon	2.72	2.99	4.44	3.25	3.92
Ileum	1.58	2.71	4.90	5.85	4.80
Stomach	1.49	1.84	7.22	7.13	11.62
Stomach contents	1.23	1.98	15.83	9.86	24.92
Tumour to tissue ratios of ^{131}I-L19-SIP					
Blood	0.48	1.00	5.45	13.54	43.44
Tongue	1.09	1.61	4.34	6.13	15.40
Sternum	2.12	3.39	9.24	12.54	20.49
Heart	1.20	2.23	11.39	27.44	59.17
Lung	1.17	1.55	6.31	11.52	22.06
Liver	2.08	4.16	16.92	41.59	81.63
Spleen	1.84	3.28	11.32	26.23	50.53
Kidney	0.68	1.30	5.50	12.06	27.88
Bladder	1.73	1.81	1.73	4.23	8.57
Muscle	5.26	7.60	21.65	45.77	103.17
Colon	2.66	2.78	4.25	3.31	5.27
Ileum	1.62	2.73	5.42	6.56	5.47
Stomach	1.41	1.73	7.01	7.32	12.67
Stomach contents	1.17	1.83	14.50	9.53	22.88

Biodistribution assessed at 3, 6, 24, 48 and 72 h after intravenous injection. Data are presented as average of four animals. Data derived from Fig. 2

Discussion

Molecular imaging of tumour angiogenesis, one of the hallmarks of cancer, has clinical perspectives for lesion detection, patient stratification, new drug development and validation, treatment monitoring and dose optimization [26]. To date, the application of PET for imaging of tumour vasculature has mostly exploited the use of radiolabelled RGD peptides for imaging of integrin $\alpha_v\beta_3$ expression, and radiolabelled peptides and MAbs for imaging VEGF/VEGFR expression [26]. Most recently the antibody fragment L19-SIP, directed against the ED-B domain of fibronectin, was identified as another attractive candidate for imaging of tumour vasculature, particularly because of its high and prolonged uptake in angiogenic tumour vessels and limited uptake in non-target organs. These targeting characteristics make L19-SIP, when armed with toxic payloads, also a promising ligand for therapy. Radioimmunotherapy is among the most advanced therapeutic approaches in the clinical development of L19-SIP, and for this purpose the antibody fragment is radiolabelled with ^{131}I [13].

After introduction of ^{131}I- and ^{99m}Tc-labelled derivatives of L19 for SPECT imaging of tumour angiogenesis [27, 28], in 2007 the first PET imaging derivative of L19-SIP was described: ^{76}Br-L19-SIP [17]. Besides clear tumour targeting, ^{76}Br-L19-SIP also showed persistent activity in blood, stomach and several other normal organs, most probably due to in vivo debromination. The ^{76}Br-L19-SIP conjugates used in these studies were slightly less stable and immunoreactive than corresponding ^{125}I-L19-SIP conjugates and appeared vulnerable for aggregate formation. The formation of free $^{76}Br^-$ due to catabolism, and its prolonged retention in blood, was also observed by Lövqvist et al., who compared the biodistribution of the ^{76}Br-38S1 and ^{125}I-38S1 antibody conjugates in tumour-bearing nude mice [29]. The aforementioned studies revealed that ^{76}Br cannot be used as a PET radionuclide substitute for iodine radioisotopes. Another limitation of ^{76}Br is its limited availability and the lack of supply of clinical grade ^{76}Br. Limited availability of long-lived positron emitters for immuno-PET made us decide a few years ago to put effort into the large-scale GMP production of ^{89}Zr (to be used for internalizing MAbs) and ^{124}I (to be used for non-internalizing MAbs) and into the development of standardized and easy-to-use radiolabelling procedures

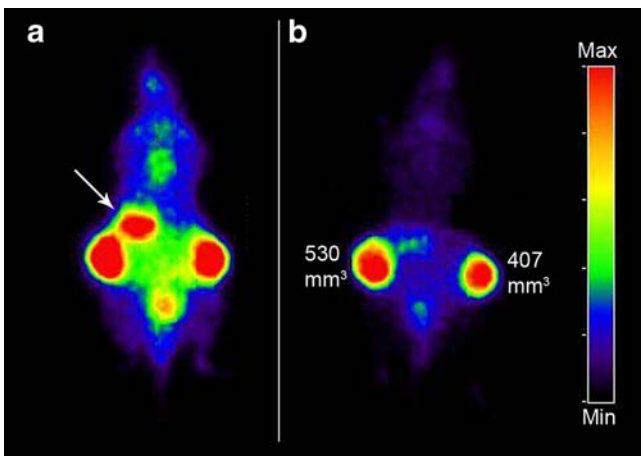

Fig. 3 PET images of FaDu xenograft-bearing nude mouse injected with ^{124}I-L19-SIP (3.7 MBq, 25 μg). Coronal images were acquired at 24 (**a**) and 48 h (**b**) after injection. Image planes have been chosen where both tumours were visible. Uptake of ^{124}I in the stomach (*arrow*) and to some extend in bladder (urine) is visible at 24 h p.i., but has disappeared at 48 h p.i.

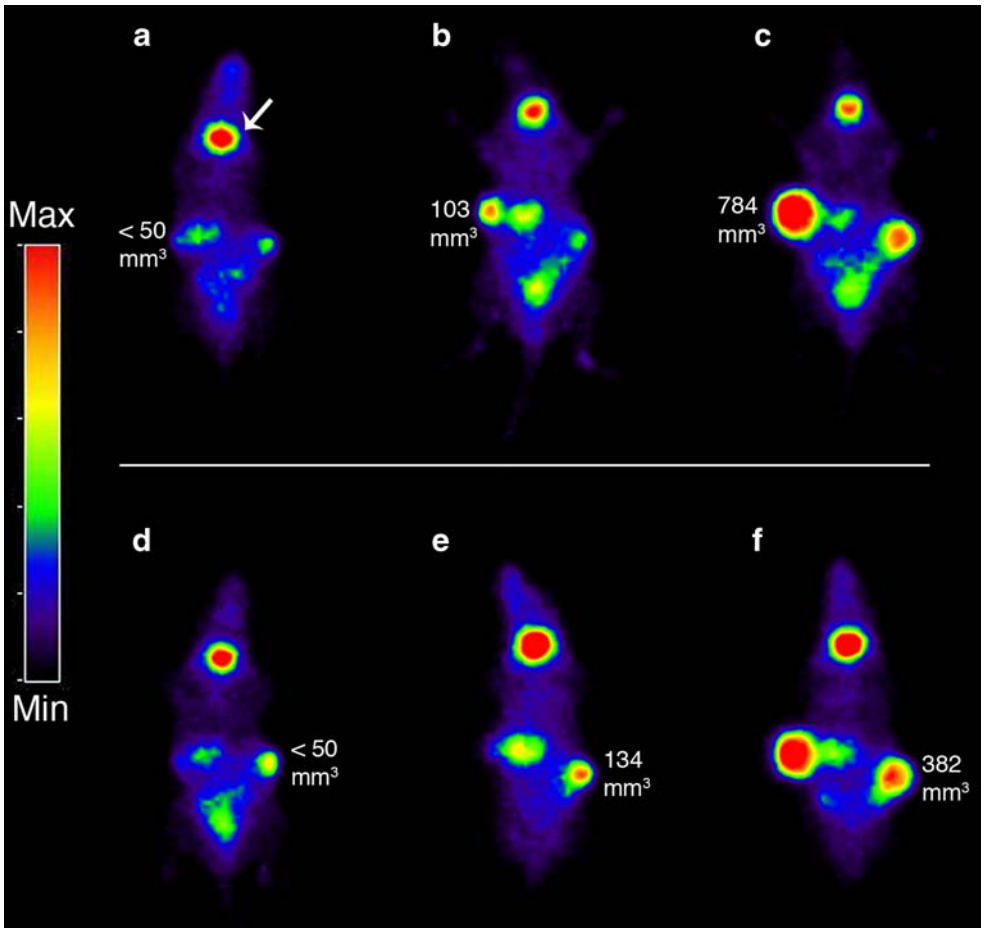

Fig. 4 Serial PET images of FaDu xenograft-bearing nude mouse injected with ^{124}I-L19-SIP (3.7 MBq, 25 μg). At 1 (**a**, **d**), 2 (**b**, **e**) and 3 (**c**, **f**) weeks after tumour implantation ^{124}I-L19-SIP was administered, and 48 h later coronal images were acquired. Image planes have been chosen where the left tumour (*upper panel*, **a**–**c**) or right tumour (*lower panel*, **d**–**f**) is optimally visible. In contrast to Fig. 3, the thyroid (*arrow*) is visible because this organ was not blocked by potassium iodide in this experiment

to facilitate the broad-scale use of immuno-PET in clinical trials [15].

In the present study, we aimed at the development of ^{124}I-L19-SIP immuno-PET, not only for imaging of tumour angiogenesis, but also as a scouting procedure prior to clinical ^{131}I-L19-SIP RIT, to confirm selective tumour targeting and to enable dosimetry. We considered ^{124}I to be the most suitable positron emitter for these applications (see "Introduction" section), but realized that availability of clinical grade ^{124}I would be a problem. The urgent need for this positron emitter also became clear from a survey performed in 2005, in which the expectations of European researchers in terms of innovative radionuclides was evaluated [30]. A questionnaire was sent to 134 nuclear medicine centres in Europe, and the 54 responding centres expressed the strongest interest in the availability of ^{124}I. This made us decide to make the production of large batches of clinical grade ^{124}I the starting point of the present studies. As demonstrated herein, infrastructure and procedures were developed for efficient GMP-compliant production of large batches of ^{124}I (>2 GBq) at high radionuclidic (>99.0%) and radiochemical (>95% as iodide) purity and low tellurium (<1 μg/ml) and endotoxin (<1.5 EU/ml) content.

Although labelling with radioiodine isotopes has been a widespread practice for decades, in several studies ^{124}I-labelled compounds were damaged and obtained in low yields [31–34]. Herein, L19-SIP was labelled with ^{124}I according to a direct labelling method with the use of a low amount of the mild oxidant IODO-GEN, and taking the I/MAb molar ratio and interference of radiolytic processes into account to arrive at optimal quality ^{124}I-L19-SIP conjugates. As convincingly shown by Fig. 1, addition of NaI as carrier to the reaction mixture during ^{124}I labelling provides a means to increase the labelling yield with this precious isotope. This carrier approach was found to be generally applicable. Of course, caution should be taken when applying these procedures for MAbs containing an overabundance of tyrosines in the complementarity-determining regions (CDR), so when the I/MAb molar ratio may be the prime parameter for immunoreactivity [35]. In that case, even single iodine incorporation on a tyrosine moiety in CDR might destroy the immunoreactivity of the MAb molecule owing to the bulkiness of the ion atom and/or change in pK_a value of the tyrosine moiety (from 10.00 to 8.51). Therefore, in this study we decided to take the I/MAb ratio not higher than strictly necessary for obtaining high labelling yields and optimal immunoreactivity. However,

when aiming the use of a ^{124}I-MAb for scouting of a ^{131}I-MAb conjugate in RIT, the I/MAb molar ratios of the conjugates can be easily synchronized, since this provides the best guarantee that the biodistribution of the therapeutic agent will be accurately predicted by the scouting agent. As another precaution to obtain optimal quality conjugates, immediately after radiolabelling ascorbic acid was added to the reaction mixture to reduce the IODO-GEN and to protect the L19-SIP against radiation damage.

L19-SIP labelled with ^{124}I according to the aforementioned procedures demonstrated optimal integrity and immunoreactivity, and exhibited the same pharmacokinetic behaviour as the corresponding ^{131}I conjugate. Moreover, biodistribution studies revealed high and selective tumour targeting, resulting in tumour to blood ratios ranging from 6.0 at 24 h to 45.9 at 72 h p.i.. Normal tissue accumulation of ^{124}I-L19-SIP was significantly lower than previously reported for ^{76}Br-L19-SIP. For example, while ^{76}Br-L19-SIP showed blood levels of 7.6±1.8 and 8.1±1.7%ID/g at 24 and 48 h p.i., respectively, for ^{124}I-L19-SIP these values were 1.37±0.43 and 0.37±0.07, respectively. As a result, high tumour to normal tissue ratios were obtained with ^{124}I-L19-SIP, resulting in clear visualization of tumours by PET imaging, even when tumours were small (~50 mm^3). These achievements will open new possibilities for ^{124}I immuno-PET in general, and for PET imaging of tumour angiogenesis with ^{124}I-L19-SIP in particular.

Acknowledgements This project was financially supported by the European Union FP6, LSHC-CT-2003-5032, ADAMANT. The publication reflects only the authors' view. The European Commission is not liable for any use that may be made of the information contained herein. The authors thank Maria J.W.D. Vosjan for her contribution to the experiments, and BV Cyclotron VU for assistance in ^{124}I production and instalment of GMP production facilities.

References

1. Neri D, Bicknell R. Tumour vascular targeting. Nat Rev Cancer 2005;5:436–46. doi:10.1038/nrc1627.
2. Rybak JN, Trachsel E, Scheuermann J, Neri D. Ligand-based vascular targeting of disease. ChemMedChem 2007;2:22–40. doi:10.1002/cmdc.200600181.
3. Carnemolla B, Balza E, Siri A, Zardi L, Nicotra MR, Bigotti A, et al. A tumor-associated fibronectin isoform generated by alternative splicing of messenger RNA precursors. J Cell Biol 1989;108:1139–48. doi:10.1083/jcb.108.3.1139.
4. Castellani P, Viale G, Dorcaratto A, Nicolo G, Kaczmarek J, Querze G, et al. The fibronectin isoform containing the ED-B oncofetal domain: a marker of angiogenesis. Int J Cancer 1994;59:612–8. doi:10.1002/ijc.2910590507.
5. Birchler MT, Milisavlijevic D, Pfaltz M, Neri D, Odermatt B, Schmid S, et al. Expression of the extra domain B of fibronectin, a marker of angiogenesis, in head and neck tumors. Laryngoscope 2003;113:1231–7. doi:10.1097/00005537-200307000-00023.
6. Ebbinghaus C, Scheuermann J, Neri D, Elia G. Diagnostic and therapeutic applications of recombinant antibodies: targeting the extra-domain B of fibronectin, a marker of tumor angiogenesis. Curr Pharm Des 2004;10:1537–49. doi:10.2174/1381612043384808.
7. Zardi L, Carnemolla B, Siri A, Petersen TE, Paolella G, Sebastio G, et al. Transformed human cells produce a new fibronectin isoform by preferential alternative splicing of a previously unobserved exon. EMBO J 1987;6:2337–42.
8. Pini A, Viti F, Santucci A, Carnemolla B, Zardi L, Neri P, et al. Design and use of a phage display library. Human antibodies with subnanomolar affinity against a marker of angiogenesis eluted from two-dimensional gel. J Biol Chem 1998;273:21769–76. doi:10.1074/jbc.273.34.21769.
9. Borsi L, Balza E, Bestagno M, Castellani P, Carnemolla B, Biro A, et al. Selective targeting of tumor vasculature: comparison of different formats of an antibody (L19) to the ED-B domain of fibronectin. Int J Cancer 2002;102:75–85. doi:10.1002/ijc.10662.
10. Berndorff D, Borkowski S, Sieger S, Rother A, Friebe M, Viti F, et al. Radioimmunotherapy of solid tumors by targeting extra domain B fibronectin: identification of the best-suited radioimmunoconjugate. Clin Cancer Res 2005;11:7053s–63s. doi:10.1158/1078-0432.CCR-1004-0015.
11. Tijink BM, Neri D, Leemans CR, Budde M, Dinkelborg LM, Stigter-van Walsum M, et al. Radioimmunotherapy of head and neck cancer xenografts using 131I-labeled antibody L19-SIP for selective targeting of tumor vasculature. J Nucl Med 2006;47:1127–35.
12. El-Emir E, Dearling JLJ, Huhalov A, Robson MP, Boxer G, Neri D, et al. Characterization and radioimmunotherapy of L19-SIP, an anti-angiogenic antibody against the extra domain B of fibronectin, in colorectal tumour models. Br J Cancer 2007;96:1862–70. doi:10.1038/sj.bjc.6603806.
13. Schliemann C, Neri D. Antibody-based targeting of the tumor vasculature. Biochim Biophys Acta 2007;1776:175–92.
14. Verel I, Visser GWM, van Dongen GAMS. The promise of immuno-PET in radioimmunotherapy. J Nucl Med 2005;46 Suppl 1:164S–71S.
15. Van Dongen GAMS, Visser GMW, Lub-de Hooge MN, De Vries EG, Perk LR. Immuno-PET: a navigator in monoclonal antibody development and applications. Oncologist 2007;12:1379–89. doi:10.1634/theoncologist.12-12-1379.
16. Boswell CA, Brechbiel MW. Development of radioimmunotherapeutic and diagnostic antibodies: an inside-out view. Nucl Med Biol 2007;34:757–87. doi:10.1016/j.nucmedbio.2007.04.001.
17. Rossin R, Berndorff D, Friebe M, Dinkelborg LM, Welch MJ. Small-animal PET of tumor angiogenesis using a 76Br-labeled human recombinant antibody fragment to the ED-B domain of fibronectin. J Nucl Med 2007;48:1172–9. doi:10.2967/jnumed.107.040477.
18. Rangan SR. A new human cell line (FaDu) from a hypopharyngeal carcinoma. Cancer 1972;29:117–21. doi:10.1002/1097-0142(197201)29:1<117::AID-CNCR2820290119>3.0.CO;2-R.
19. Qaim SM, Hohn A, Bastian T, El-Azoney KM, Blessing G, Spellerberg S, et al. Some optimisation studies relevant to the production of high-purity 124I and 120gI at a small-sized cyclotron. Appl Radiat Isot 2003;58:69–78. doi:10.1016/S0969-8043(02)00226-9.
20. Monograph 01/2008:2314 sodium iodide (123I) solution for radiolabeling. European Pharmacopoeia. Strasbourg: European Directorate for the Quality of Medicines & HealthCare (EDQM); 2007:1010.
21. Verel I, Visser GWM, Vosjan MJWD, Finn R, Boellaard R, van Dongen GAMS. High-quality 124I-labelled monoclonal antibodies

for use as PET scouting agents prior to 131I-radioimmunotherapy. Eur J Nucl Med Mol Imaging 2004;31:1645–52. doi:10.1007/s00259-004-1632-8.
22. Qiu-e C, Zhide H, Zubi L, Jialin W, Qiheng X. Highly sensitive spectrophotometric determination of trace amounts of tellurium (IV) with the tungstate-basic dyes-poly(vinyl alcohol) system. Analyst (Lond) 1998;123:695–7. doi:10.1039/a707722j.
23. Visser GWM, Klok RP, Klein-Gebbink JW, Ter Linde T, Van Dongen GAMS, Molthoff CF. Optimal quality (131)I-monoclonal antibodies on high-dose labeling in a large reaction volume and temporarily coating the antibody with IODO-GEN. J Nucl Med 2001;42:509–19.
24. de Jong HWAM, van Velden FHP, Kloet RW, Buijs FL, Boellaard R, Lammertsma AA. Performance evaluation of the ECAT HRRT: an LSO-LYSO double layer high resolution, high sensitivity scanner. Phys Med Biol 2007;52:1505–26. doi:10.1088/0031-9155/52/5/019.
25. Comtat C, Bataille F, Michel C, Jones JP, Sibomana M, Janeiro L, et al. OSEM-3D reconstruction strategies for the ECAT HRRT. IEEE NSS Conf Rec 2004;6:3492–6.
26. Cai W, Chen X. Multimodality molecular imaging of tumor angiogenesis. J Nucl Med 2008;48:113S–28S. doi:10.2967/jnumed.107.045922.
27. Santimaria M, Moscatelli G, Viale GL, Giovannoni L, Neri G, Viti F, et al. Immunoscintigraphic detection of the ED-B domain of fibronectin, a marker of angiogenesis, in patients with cancer. Clin Cancer Res 2003;9:571–9.
28. Berndorff D, Borkowski S, Moosmayer D, Viti F, Müller-Tiemann B, Sieger S, et al. Imaging of tumor angiogenesis using 99mTc-labeled human recombinant anti-ED-B fibronectin antibody fragments. J Nucl Med 2006;47:1707–16.
29. Lövqvist A, Sundin A, Alström H, Carlsson J, Lundqvist H. Pharmacokinetics and experimental PET imaging of a bromine-67-labeled monoclonal anti-CEA antibody. J Nucl Med 1997;38:395–401.
30. Barbet J, Chatal JF, Gauche F, Martino J. Which radionuclides will nuclear medicine need tomorrow? Eur J Nucl Med Mol Imaging 2006;33:627–30. doi:10.1007/s00259-006-0116-4.
31. Finn R, Cheung NKV, Divgi C, St Germain J, Graham M, Pentlow K, et al. Technical challenges associated with the radiolabeling of monoclonal antibodies utilizing short-lived, positron emitting radionuclides. Int J Rad Appl Instrum B 1991;18:9–13.
32. Lee FT, Hall C, Rigopoulos A, Zweit J, Pathmaraj K, O'Keefe GJ, et al. Immuno-PET of human colon xenograft-bearing BALB/c nude mice using 124I-CDR-grafted humanized A33 monoclonal antibody. J Nucl Med 2001;42:764–9.
33. Collingridge DR, Carroll VA, Glaser M, Aboagye EO, Osman S, Hutchinson OC, et al. The development of [124I]iodinated-VG76e: a novel tracer for imaging vascular endothelial growth factor in vivo using positron emission tomography. Cancer Res 2002;62:5912–9.
34. Glaser M, Collingridge DR, Aboagye EO, Bouchier-Hayes L, Hutchinson OC, Martin SJ, et al. Iodine-124 labelled annexin-V as a potential radiotracer to study apoptosis using positron emission tomography. Appl Radiat Isot 2003;58:55–62. doi:10.1016/S0969-8043(02)00239-7.
35. Nikula TK, Bocchia M, Curcio MJ, Sgouros G, Ma Y, Finn RD, et al. Impact of the high tyrosine fraction in complementarity determining regions: measured and predicted effects of radiodination on IgG immunoreactivity. Mol Immunol 1995;32:865–72. doi:10.1016/0161-5890(95)00052-G.